

# Diamonds in HD 97048: a closer look

E. Habart, L. Testi, A. Natta, M. Carillet<sup>1</sup>

*INAF-Osservatorio Astrofisico di Arcetri, Largo E. Fermi 5, 50125 Firenze, Italy*

habart@arcetri.astro.it, lt@arcetri.astro.it, natta@arcetri.astro.it,  
marcel@arcetri.astro.it

## ABSTRACT

We present adaptive optics high angular resolution ( $\sim 0''.1$ ) spectroscopic observations in the  $3\ \mu\text{m}$  region of the Herbig Ae/Be star HD 97048. For the first time, we spatially resolve the emission in the diamond features at  $3.43$  and  $3.53\ \mu\text{m}$  and in the adjacent continuum. Using both the intensity profiles along the slit and reconstructed two-dimensional images of the object, we derive full-width at half-maximum sizes consistent with the predictions for a circumstellar disk seen pole-on. The diamond emission originates in the inner region ( $R \lesssim 15$  AU) of the disk.

*Subject headings:* instrumentation : adaptive optics - stars: pre-main sequence - stars : individual (HD 97048) - circumstellar matter - dust, extinction - ISM : lines and bands

## 1. Introduction

HD 97048 is a Herbig Ae/Be star, member of the Chamaeleon I association, situated at 180 pc (van den Ancker et al. 1997; Whittet et al. 1997). Thé et al. (1986) derived from a photometric and spectroscopic study of HD 97048 that its infrared (IR) excess originates in a flattened shell structure or disk of dust particles seen pole-on. The unresolved SEST image of HD 97048 taken by Henning et al. (1998) together with the measured mm-flux also points towards the presence of a flattened disk-like structure (Henning et al. 1993, 1998). The object is not extended in the near-IR on scales of  $\lesssim 1''$  (Henning et al. 1998), but it is in the mid-IR on scales of  $5\text{-}10''$  (Prusti et al. 1994; Siebenmorgen et al. 2000). The mid-IR

---

<sup>1</sup>On move to Laboratoire Universitaire d'Astrophysique de Nice, UMR 6525 du CNRS, Parc Valrose, 06108 Nice Cedex 2, France

emission, dominated by aromatic infrared emission bands (Siebenmorgen et al. 2000), is most probably due to an extended envelope of transiently heated very small grains and Polycyclic Aromatic Hydrocarbons (PAHs). However, van Boekel et al. (2004) have recently spatially resolved the  $10\ \mu\text{m}$  emission of the central source, showing that most of the emission in the  $8.6$ ,  $11.3$  and  $12.7\ \mu\text{m}$  features comes in fact from a region of  $1.2$ - $1.6''$  or  $200$ - $300$  AU, very likely a disk.

The spectra of HD 97048 show, next to the infrared emission bands at  $3.3\ \mu\text{m}$  attributed to PAHs, the rare emission features at  $3.43$  and  $3.53\ \mu\text{m}$  (e.g., Blades & Whittet 1980; Guillois et al. 1999; Van Kerckhoven et al. 2002). Guillois et al. (1999) proposed to attribute these bands to diamond surface C-H stretching features; an identification which, because of the good match between laboratory and observed spectra, is very persuasive. Nanodiamonds are the most abundant presolar grains in primitive meteorites, and they could in fact constitute an important component of the dust in circumstellar environments and in the interstellar medium (e.g., Jones et al. 2004). However, the diamond particles in HD 97048 or Elias 1 are probably much larger (size of  $\sim 10$ – $50$  nm or larger) than the “true” nanodiamonds (mean sizes of the order of  $2$ – $3$  nm) observed in primitive meteorites (Jones et al. 2004).

One way to better understand the properties and evolution of diamond particles is to study the spatial distribution of their emission. Presently, the only observational constraints one has come from speckle observations by Roche et al. (1986) who found that the emission in the  $3.53\ \mu\text{m}$  band in HD 97048 is unresolved and arises from a region  $< 0''.1$  in diameter. Here, we present adaptive optics high angular resolution ( $\sim 0''.1$ ) spectroscopic observations of HD 97048. These observations allow us to spatially resolve for the first time the  $3\ \mu\text{m}$  features attributed to diamonds, as well as the adjacent continuum. In Sect. 2, we present the observations. The results are presented in Sect. 3 and discussed in Sect. 4.

## 2. Observations and data reduction

Long slits spectra in the L-band ( $3.2$ – $3.76\ \mu\text{m}$ ) of HD 97048 were taken on 10 January 2003 with the adaptive optics (AO) system NAOS-CONICA (NACO) at the VLT, using the visible  $14\times 14$  Shack-Hartmann wave-front sensor working at nearly 500 Hz. The  $28''$  long slit had a width of  $0''.086$  which roughly corresponds to the diffraction limit while the pixel scale was  $\sim 0''.0547$  and the spectral resolution  $\sim 700$ . We took 7 slit positions: one centered on the star and the others at  $0''.043$ ,  $0''.086$ ,  $0''.129$  and  $-0''.043$ ,  $-0''.086$ ,  $-0''.129$  off axis. For each slit position, in order to correct from the atmospheric and instrumental background, we employed standard chop/nod technique with a throw of  $\sim 9''$  in the north-south direction. The integration time per chop- or nod-positions was 1 min.

The log of the observational conditions reports a Fried parameter  $r_0$  close to 10 cm (at 500 nm), an average outer-scale  $\mathcal{L}_0$  of  $\sim 15$  m, and a resulting average coherent energy (after AO correction and at  $2.2 \mu\text{m}$ ) of up to 40% on axis. The latter roughly gives the actual Strehl ratio characterizing the quality of our data. According to simultaneous measurements, the seeing (at 500 nm) was  $\sim 1''.1$  consistent with the NACO values. Our observations clearly benefit from good seeing conditions and AO correction, and the achieved angular resolution was close to the diffraction limit.

Data reduction was performed using firstly a standard procedure for IR spectroscopic observations (pre-processing phase), and then a classical Richardson-Lucy (LR) deconvolution method. During the pre-processing phase, to remove the telluric features we used the observations of a spectroscopic standard star (HIP 53074) taken on 20 February 2003, with the same airmass. For the deconvolution procedure, and to have a suitable estimate of the point-spread function (PSF), we used instead a second reference star (HIP 20440), observed on 19 January 2003, which provided a better match to our object in terms of atmospheric turbulence conditions ( $r_0$ ,  $\mathcal{L}_0$ , seeing), and AO correction quality (K-band Strehl ratio  $\sim 30\%$ ).

### 3. Results

#### 3.1. Spectra

Fig. 1 shows the spectrum obtained by combining all the slits and for distances from the star going from 0 to  $1''$ . It clearly shows the two strong features at  $3.43$  and  $3.53 \mu\text{m}$ , attributed to diamonds. The features are not smooth, but show a number of components, in particular, the  $3.41$ ,  $3.43$ ,  $3.50$ ,  $3.51$  and  $3.53 \mu\text{m}$  ones. These characteristics support the identification of the carriers of the two features as diamonds (e.g., Guillois et al. 1999; Van Kerckhoven et al. 2002; Jones et al. 2004). The spectrum shows also a weaker feature at  $3.3 \mu\text{m}$ , characteristic of PAHs. There may be also some hydrogen emission lines; the Pf  $\delta$  on top of the broad PAH feature at  $3.3 \mu\text{m}$  and the Pf  $\gamma$  line at  $3.74 \mu\text{m}$ .

In Fig. 1, we also compare our spectrum with that obtained with the Short Wavelength Spectrometer (SWS) on board the Infrared Space Observatory (ISO) with a slit of  $20 \times 33''$ . The ISO-SWS spectrum contains both the disk and emission from the reflection nebula that surrounds the system (Siebenmorgen et al. 2000; van Boekel et al. 2004). Comparing the two spectra, we see that the diamond components are very similar in peak position, width and relative strength. Moreover, the peak/continuum ratio in the diamond bands is roughly similar. This suggests that diamond emission is confined to the disk. On the other hand,

the ISO spectrum shows stronger PAH emission at  $3.3 \mu\text{m}$  than the NACO one, consistent with the hypothesis that the PAH feature seen in the ISO spectrum comes from both the disk and the surrounding nebula (van Boekel et al. 2004).

## 3.2. Brightness spatial distribution

### 3.2.1. Along the slit

Fig. 2 shows the intensity profile (after continuum subtraction) of the two  $3.43$  and  $3.53 \mu\text{m}$  features along the slit length. The intensity profile in the slit centered on the star and at  $0''.043$  have been averaged together because the star was offset by approximately  $1/4$  of slit (i.e.,  $\sim 0.02''$ , see Fig. 4). Fig. 2 also shows the intensity profile of the continuum (measured between  $3.6$  and  $3.7 \mu\text{m}$ ) and of the observed reference star (the assumed PSF). The spatial extent of the diamond emission in both the  $3.43$  and  $3.53 \mu\text{m}$  features is significantly broader than that of the continuum, which is slightly broader, in turn, than the PSF. Note that since the PSF data resulted in a slightly worse Strehl ratio (see Sect. 2) than the object data, it is unlikely that the apparent extension of the continuum is due to an additional broadening from the combination of atmospheric conditions and partial AO correction. The PAH emission appears to be more extended than the diamond features; it will be discussed in details in a forthcoming paper presenting other NACO observations of the  $3.3 \mu\text{m}$  PAH emission band in Herbig Ae/Be stars.

As discussed above, the fact that both the diamond features and the continuum emission are resolved is clearly visible already in the pre-processed data. Nevertheless, in order to better estimate the exact spatial extensions and eliminate, as far as possible, the remaining atmospheric and post-AO broadening effects on the profiles, we have applied to the data a classical LR deconvolution method. In practice this was performed using the Software Package AIRY (Correia et al. 2002). In order to avoid Gibbs oscillations (also known as “ringing” effect – see Bertero & Boccacci 1998) in the rather flat central feature of the data at  $3.43$  and  $3.53 \mu\text{m}$  we have stopped our LR iterative method after 10 iterations, while for the continuum data we have performed a maximum of 100 iterations since no ringing effect appeared <sup>1</sup>.

The results are shown in Fig. 3, from which we derive a full-width at half-maximum (FWHM) of  $0''.18$  (or 32 AU) for the diamond features, and of  $0''.13$  (or 23 AU) for the con-

---

<sup>1</sup>Note that stopping the continuum reconstruction at 10 iterations would not essentially change the result in terms of resulting FWHM (difference less than 5%).

tinuum emission. These results are consistent with a simple quadratic subtraction assuming Gaussian light distribution in the pre-processed data. The signal-to-noise ratio on the spatiole emission profiles is very high (greater than 100) and the theoretical error on the FWHM from gaussian fits is less than 1%. This is clearly an underestimate of the real uncertainties of our measurement. Errors on the FWHM values are dominated by systematic errors at the level of 10 to 20%. The spatial extension derived here for the 3.53  $\mu\text{m}$  band is larger by almost a factor of 2 than the upper limit inferred by Roche et al. (1986). However, the 3.53  $\mu\text{m}$  emission feature is spatially unresolved in their speckle observations performed at the Anglo-Australian 3.9-m telescope (with a diffraction limit of  $\gtrsim 0''.2$ ). The derived upper limit assumes an amount of super-resolution (see e.g., Anconelli et al. 2004) that is hardly compatible with the modest signal-to-noise ratio caused by a seeing value of  $3''$  and no AO correction. On the contrary, the spatial extension we derive here is approximately twice the diffraction-limit of the 8.2-m VLT. Nevertheless, further accurated AO-assisted 2D imaging with NACO should be performed to confirm our size estimates.

### 3.2.2. 2D intensity maps: the disk is resolved

Because of the way the slits were positioned and the chop/nod procedure used, we have a 2D coverage of the plane of the sky for a region of  $0.26 \times 4''$ , about  $47 \times 720$  AU. Fig. 4 shows the map of the emission of the 3.43 and 3.53  $\mu\text{m}$  features and of the continuum. These maps were obtained by deconvolving independently the data obtained for each of the 7 slit positions, and hence recomposing the 7 slit vectors into 8 resulting pixels (each slit was shifted by a value that is half the width of the slit itself during the observations).

Both in the features and in the continuum, the emission is roughly spherical, with FWHM sizes of about  $0.18 \times 0.18''$ ,  $32 \times 32$  AU in the features, and  $0.13 \times 0.13''$ ,  $23 \times 23$  AU in the continuum, as derived in Sect. 3.2.1 from the analysis of the central slits. The slight difference between the 3.43 and 3.53 band maps is not significant, given the uncertainties of the data.

## 4. Discussion and conclusions

Our NACO/VLT observations allow us to resolve for the first time the emission in the diamond features (and the adjacent continuum) in a pre-main-sequence star. The FWHM sizes we derive are typical of emission arising in a circumstellar disk, as we will see in the following; the roughly spherical shape of the emission maps confirms the hypothesis of a

pole-on disk in HD 97048 put forward by Thé et al. (1986).

Models of the intensity profile expected from flared circumstellar disks around Herbig Ae/Be stars, similar to HD 97048, have been recently computed by Habart et al. (2004). The models include large grains, in thermal equilibrium with the stellar radiation field, as well as transiently heated small graphite grains and PAHs, but not diamonds. These models show that the continuum emission at  $\sim 3 \mu\text{m}$  is dominated by warm large (size of  $\sim 0.1 \mu\text{m}$ ) grains at thermal equilibrium; when convolved with a PSF of  $\text{FWHM} \sim 0.1''$ , the intensity profile is only slightly bigger than the PSF, as in our observations.

In all models, the emission of transiently heated particles is significantly broader than that of the large grains at the same frequency. This is easily understood when considering the different excitation mechanism, and is discussed in details in Habart et al. (2004). In fact, there is evidence in HD 97048 that the mid-IR PAH emission is extended on a scale of  $1.2\text{-}1.6''$  or  $200\text{-}300 \text{ AU}$  (van Boekel et al. 2004), comparable to the outer disk radii seen at millimeter wavelengths in similar systems (Mannings & Sargent 1997). The more extended emission seen by Siebenmorgen et al. (2000) must come, instead, from a surrounding nebula.

The diamond emission is extended more than the continuum emission, but less than the PAH emission. This is roughly consistent with the idea that the diamond carrier of the  $3 \mu\text{m}$  features observed in HD 97048 have sizes intermediate between those of large grains and of PAHs, as suggested by detailed analysis of the ISO spectrum (see e.g. Van Kerckhoven et al. 2002; Sheu et al. 2002; Jones et al. 2004). Self consistent models which explore the effect of diamond properties and disk geometry are required to make a useful comparison with observations.

The results presented in this letter add an important piece of information to the studies of the properties of circumstellar disks and of the nature of the solid particles they contain. For the first time, we were able to resolve the inner disk emission in the Herbig Ae/Be star HD 97048, to show that the disk is seen pole-on, confirming previous indirect evidence, to resolve the rare emission in the two features at  $3.43$  and  $3.54 \mu\text{m}$  attribute to diamonds and to prove beyond doubts their origin in the inner region ( $R \lesssim 15 \text{ AU}$ ) of the disk.

Based on observations collected at the European Southern Observatory, Chile, ESO N. 70.C-0659.

## REFERENCES

- Anconelli, B, Bertero, M, Boccacci, P, & Carbillet, M. 2004, *submitted to A&A*.
- Bertero, M & Boccacci, P. 1998, *Introduction to Inverse Problems in Imaging, IOP Publishing, Bristol*.
- Blades, J. C & Whittet, D. C. B. 1980, *MNRAS*, 191:701.
- Correia, S, Carbillet, M, Boccacci, P, Bertero, M, & L.Fini. 2002, *A&A*, 387:733.
- Geballe, T. R, Noll, K. S, Whittet, D. C. B, & Waters, L. B. F. M. 1989, *ApJ*, 340:L29.
- Guillois, O, Ledoux, G, & Reynaud, C. 1999, *ApJ*, 521:L133.
- Habart, E, Natta, A, & Krugel, E. 2004, *A&A, in press, astro-ph/0405195*.
- Henning, T, Pfau, W, Zinnecker, H, & Prusti, T. 1993, *A&A*, 276:129.
- Henning, T, Burkert, A, Launhardt, R, Leinert, C, & Stecklum, B. 1998, *A&A*, 336:565.
- Jones, A. P, d’Hendecourt, L. B, Sheu, S. Y, Chang, H. C, Cheng, C. L, & Hill, H. G. M. 2004, *A&A*, 416:235.
- Mannings, V.M. & Sargent, A.I. 1997, *ApJ*, 490:792.
- Prusti, T, Natta, A, & Palla, F. 1994, *A&A*, 292:593.
- Roche, P. F, Allen, D. A, & Bailey, J. A. 1986, *MNRAS*, 220:7.
- Sheu, S. Y, Lee, I. P, Lee, Y. T, & Chang, H. C. 2002, *ApJ*, 581:L55.
- Siebenmorgen, R, Prusti, T, Natta, A, & Muller, T. G. 2000, *A&A*, 361:258.
- Thé, P. S, Tjin, H. R. E, Steenman, H, & Wesselius, P. R. 1986, *A&A*, 155:347.
- van Boekel, R, Waters, L. B. F. M, Dominik, C, Dullemond, C. P, Tielens, A. G. G. M, & De Koter, A. 2004, *A&A*, 418:177.
- van den Ancker, M. E, The, P. S, Tjin A Djie, H. R. E, Catala, C, De Winter, D, Blondel, P. F. C, & Waters, L. B. F. M. 1997, *A&A*, 324:L33.

Van Kerckhoven, C, Tielens, A. G. G. M, & Waelkens, C. 2002, *A&A*, 384:568.

Whittet, D. C. B, Prusti, T, Franco, G. A. P, Gerakines, P. A, Kilkenny, D, Larson, K. A,  
& Wesselius, P. R. 1997, *A&A*, 327:1194.



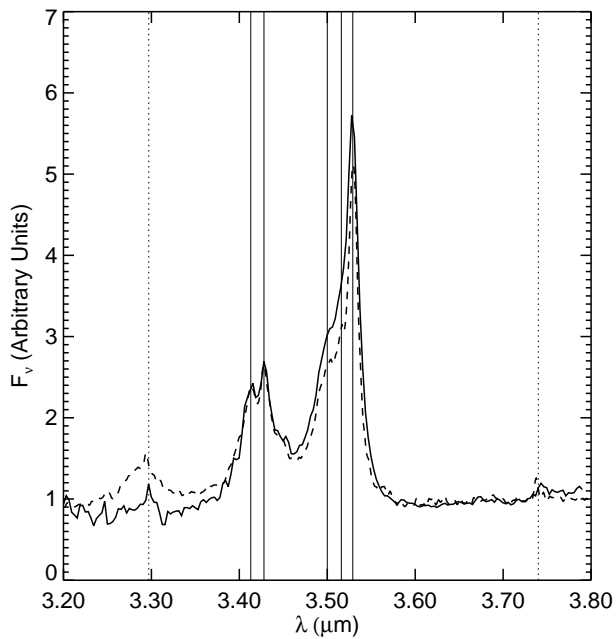


Fig. 1.— Spectrum obtained by combining all the slits and for distances from the star going from 0 to 1'' (solid lines). The dashed line shows the ISO-SWS spectrum, obtained with a beam of  $20 \times 33''$ . We also show as solid vertical lines the diamond feature positions and as vertical dotted lines the position of the Pf  $\delta$  line (on top of the broad PAH feature at  $3.3 \mu\text{m}$ ) and the Pf  $\gamma$  line at  $3.74 \mu\text{m}$ .

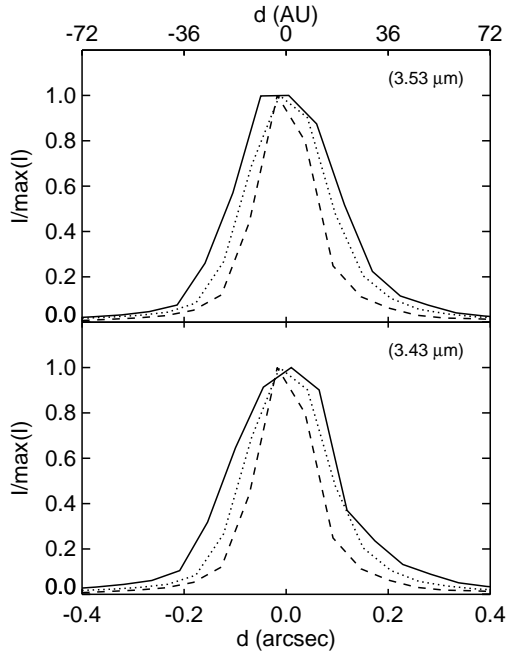


Fig. 2.— Normalized spatial emission profiles of the stronger 3.43 and 3.53  $\mu\text{m}$  diamond features (continuum subtracted, solid lines) as function of the distance from the star. The scale on the lower axis shows the distance in arcsec, that on the upper axis the corresponding value in AU. Dotted and dashed lines show the intensity profile of the continuum and of the PSF, respectively.

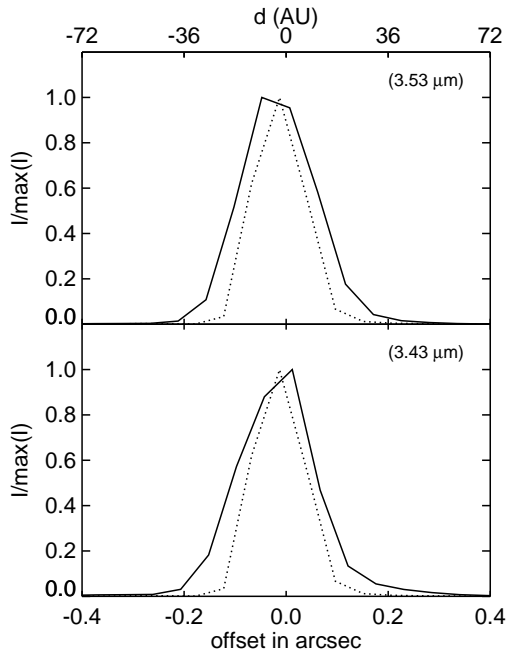


Fig. 3.— Deconvolved normalized emission profiles of the stronger diamond features (continuum subtracted, solid lines) and of the continuum (dotted lines) obtained using a classical LR method (see text for details). The scale on the lower axis shows the distance in arcsec, that on the upper axis the corresponding value in AU.

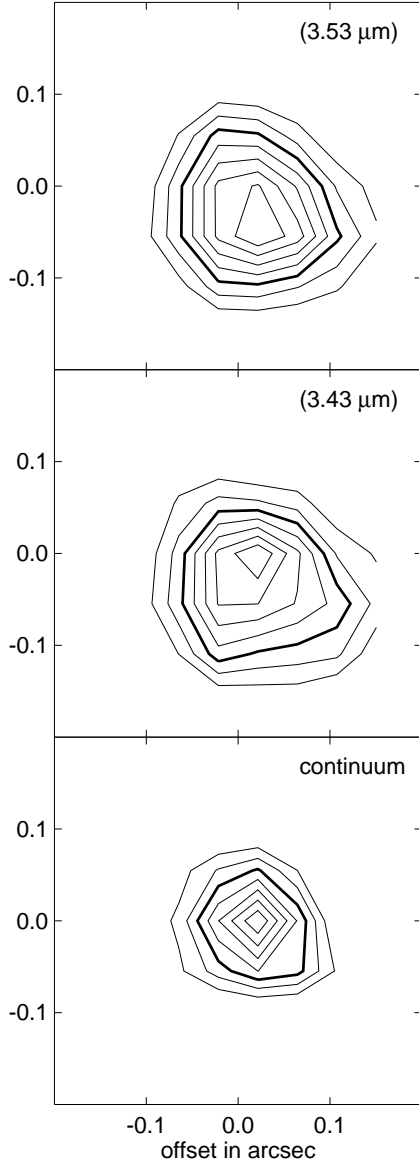


Fig. 4.— Deconvolved normalized emission map of the 3.43 and 3.53  $\mu\text{m}$  features (continuum subtracted) and of the continuum. The contour levels go from 0.3 to 0.9 (step=0.1); the 0.5 level is shown in thick line.